High dynamic range optical coherence tomography angiography (HDR-OCTA)

Xiang Wei,[1,2] Tristan T. Hormel,[1] Shaohua Pi,[1] Yukun Guo,[1] Yifan Jian,[1,2] and Yali Jia[1,2,*]

[1]*Casey Eye Institute, Oregon Health & Science University, Portland, OR, 97239, USA*
[2]*Department of Biomedical Engineering, Oregon Health & Science University, Portland, OR, 97239, USA*
*jiaya@ohsu.edu

Abstract: The dynamic range of current optical coherence tomography (OCT) angiography (OCTA) images is limited by the fixed scanning intervals. High speed OCT devices introduce the possibility of extending the flow signal dynamic range. In this study, we created a novel scanning pattern for achieving high dynamic range (HDR)-OCTA with a superior scanning efficiency. We implemented a bidirectional, interleaved scanning pattern that is sensitive to different flow speeds by adjustable adjacent inter-scan time intervals. We found that an improved flow dynamic range can be achieved by generating 3 different B-scan time intervals using 3 repetitions.

1. Introduction

Optical coherence tomography (OCT) angiography (OCTA) is a non-invasive modality for imaging retinal and choroidal blood flow [1–4]. Compared to conventional fluorescein angiography, it does not require dye injection and so avoids deleterious, and sometimes serious, side-effects [5]. Many OCTA algorithms have been developed; they generate depth-resolved angiograms by measuring the variation of OCT signal due to blood flow induced signal change among subsequent images. It can be computed based on the phase [3,6], amplitude [1,4], or both parts (complex OCTA) [2,7] of the OCT signal. Image acquisition speed is a paramount performance parameter in OCT systems. The speed of commercially available OCT systems is up to 100-kHz, but experimental OCT systems have pushed into megahertz A-scan rates [8]. Fast OCT systems have many benefits. Shorter scanning times reduce the incidence of motion artifacts. They enable measurements with both a larger field of view (FOV) and make denser scanning possible, which allows high resolution in widefield OCT systems. However, higher scanning speeds may also decrease the sensitivity of the OCT system and lead to further artifacts that disturb OCTA image quality [9].

Previous studies have shown OCTA flow signal is affected by the time interval between consecutive B-scans [2,10–12]. If the inter-scan time is large, the OCTA signal saturates easily for low flow velocities, and vessels carrying blood at different speeds might appear at the same signal level. In contrast, a short inter-scan time can better distinguish the different flow rate between vessels carrying fast flow; however, short inter-scan times have reduced sensitivity to slow flow, as the red blood cells do not have sufficient time to move far enough within capillaries to produce a detectable speckle variance [13]. The ability to better quantify flow magnitude in particular represents a major aspiration for OCTA technology. Currently, commercial instruments and most OCTA studies are limited in scope to simply quantifying vascular patterns and organization, without the ability to make velocimetric measurements. There are indications in both diabetic retinopathy (DR) [14] and age-related macular degeneration (AMD) [15] that flow impairment occurs during disease progression, and previous work has established flow impairment adjacent to regions of geographic atrophy [11,16]. There is, then, reason to believe that flow magnitude is clinically significant. Without

a reliable method to measure flow speed frequently and rigorously *in vivo*, we simply don't know to what extent changes in flow may be indicative of disease progression. It is possible that we may gain access to a host of biomarkers and indicators for treatments if we gain the ability to measure flow magnitude, even if they are still limited in the sense of being relative flow measurements.

Maintaining sensitivity to slow flow while increasing the flow signal dynamic range is therefore an active topic in OCTA, and success in both aims will generate new applications relating to the detection of pathologies associated with flow rates. In photography, the dynamic range of an image can be affected by the sensitivity and noise level of the detector. Multi-exposure high dynamic range photography is an attempt to overcome this issue [17]. It is based on the observation that the dynamic range of an image sensor is correlated to its exposure time. By combining long and short exposure images, the dynamic range of the combined image can be expanded [18]. For OCTA, the scanning interval is analogous to the exposure time in photography. By combining short with long inter-scan times, a high dynamic range (HDR)-OCTA image can be generated.

Many previous research works have demonstrated different scanning methods to decrease noise [19], increase efficiency [20,21] or increase the velocity ranging in OCT applications [22,23]. Recently, a pilot version of HDR-OCTA, variable inter-scan time analysis (VISTA), demonstrated sufficient sensitivity to detect flow impairment before the onset of capillary dropout [16]. However, this prior work was based on an inefficient OCT scanning protocol that had to achieve the optimal duty cycle by including an unnecessary fly-back at every B-scan across the fast scanning priority axis, and an additional superfluous cross-sectional B-scan. A novel fly-backless bidirectional scanning pattern has been introduced by Ju, et al. which can increase scanning efficiency [20]. Based in part on this, for HDR-OCTA we have devised a bidirectional, interleaved scanning protocol can achieve an optimal scanning duty cycle and obtain three different inter-B-scan intervals with only three repetitions as opposed with the method used in previous work [11] could form two intervals with three repetitions.

2. Method

2.1 Amplitude based OCTA signal processing

Split-spectrum amplitude-decorrelation angiography (SSADA) is a commercialized OCTA algorithm [24] that offers superior angiogram image contrast and quality. The flow signal in SSADA is extracted using the decorrelation value from each of several spectrums split from the entirety of the signal generated by repeated B-scans. The application of the split-spectrum approach improves the signal to noise ratio of OCTA images and the flow tissue contrast. The fundamental theory of SSADA can be expressed as [1]

$$\bar{D}_{SSADA}(x,z) = 1 - \frac{1}{N-1} \cdot \frac{1}{M} \sum_{n=1}^{N-1} \sum_{m=1}^{M} \frac{A_{n,m}(x,z) \cdot A_{n+1,m}(x,z)}{\frac{1}{2} A_{n,m}(x,z)^2 + \frac{1}{2} A_{n+1,m}(x,z)^2}. \quad (1)$$

Here, the decorrelation signal $\bar{D}_{SSADA}$ is calculated as an average over the N repeats for each scanning location and the M divisions of the full spectrum. For each split-spectrum at each repeat, the autocorrelation with the subsequent scan is calculated using OCT intensity signals $A_n(x,z) \cdot A_{n+1}(x,z)$. According to a previous study, the autocorrelation of the laser speckle signal $g(\tau)$ can be represented as [25]

$$g(\tau) = I^2 \cdot \exp\left(-\frac{|\tau|}{\tau_c}\right). \quad (2)$$

Here, τ is the exposure time and I is the amplitude of the speckle signal, which in OCTA can be correlated to the scanning interval. τ_c is the correlation coefficient, which can be related to the flow speed v_{flow}, bulk motion v_{bulk} and Brownian motion $v_{browian}$, according to

$$\tau_c \cdot (v_{flow} + v_{brownian} + v_{bulk}) = k, \tag{3}$$

where we assume τ_c obeys a linear relationship with the motion. Thus,

$$g_g(\tau) = I^2 \cdot \exp\left[-\frac{\tau \cdot (v_{flow} + v_{brownian} + v_{bulk})}{k}\right]. \tag{4}$$

k is a constant. Here τ actually represents the scanning interval, which is equivalent to the exposure time in Eq. (2). Equation (1) can then be written

$$\bar{D}_{SSADA} = 1 - \exp\left[-\frac{\tau \cdot (v_{flow} + v_{brownian} + v_{bulk})}{k}\right]. \tag{5}$$

So, the relationship between the SSADA signal and the flow is an exponential relationship. The sensitivity of v_{flow} is related to the scanning interval τ, and also the dynamic range or the linearity of $\bar{D}_{SSADA}$ is determined by τ.

Conventional OCTA systems use a raster scanning pattern in which the scanning interval between each repeat is fixed and cannot be changed during data acquisition. This usually results in a narrow flow signal dynamic range. Therefore, conventional OCTA doesn't carry much flow rate information and only infrequently used to make velocimetric measurements. To generate HDR-OCTA images reflecting blood flow rate, a high-speed OCT system and a novel multi-interval scanning method will be described below.
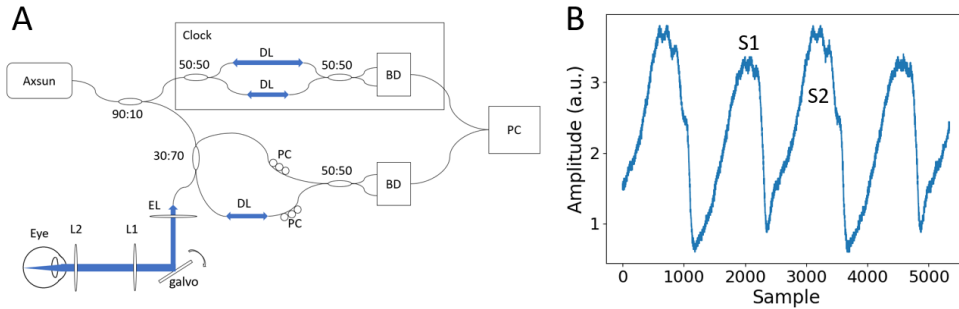
2.2 400k swept source (SS)-OCT system

Fig. 1. (A) System configuration for the 400-kHz SS-OCT system that contains two 200-kHz multiplexed swept sources. BD is balanced detector, PC is polarization controller, DL is delay line, L1 is 100 mm focus lens, L2 is 50 mm focus lens and EL is the electric lens. (B) Spectrum of the 400-kHz AXSUN laser, where S1 and S2 are the spectra of the individual 200-kHz swept sources.

A custom-built SS-OCT system (Fig. 1(A)) using 400-kHz swept source laser (AXSUN Technologies) with center wavelength of 1060 nm and 100 nm bandwidth was used in this study. Two 200-kHz swept laser engines with 50% duty cycles were combined to achieve a total swept rate of 400-kHz with 100% duty cycle (Fig. 1(B)). The laser engine doesn't contain a built-in k-space clock (k-clock) signal output, so a Mach-Zehnder interferometer was built using 10% of the output power from the laser to provide the high-speed k-clock, linearly sampling the spectrum in k-space. A 70:30 optic coupler was used to split the power to the reference and sample arm. The optical power on the pupil can be controlled with a

variable attenuator and was set to 2 mW. The data was acquired using a 1.8 GS/s ATS9360 (Alazar, Inc.) digitizer and 1 GHz balanced detectors (Thorlabs, Inc.). A 3-mm galvo scanner (ScannerMax) was used to scan the laser beam. The axial resolution of 5.5 µm and the imaging depth of 4.2 mm in the air were achieved by sampling across the total 100 nm bandwidth with 1536 sampling points. The beam size on the pupil is 1.2 mm and the lateral resolution is 19 μ m. The power and spectrum shape of the two lasers are slightly different (Fig. 1(B)); during data processing, data acquired from each laser was processed separately. The sensitivity of this system was measured to be 120 dB. A real-time GPU-based OCT display and data acquisition software were also developed for this system [26].

2.3 Bidirectional scanning protocols opts out of fly-back time

OCT scanning of the retina is commonly performed using a raster scan pattern by applying a sawtooth voltage function on the galvanometer mirror for the fast-axis and a step function for the slow-axis. The most commonly used scanner is based on two galvo motors precisely driving reflection mirrors. The galvo motors have a response time which is limiting the maximum resonant frequency. Therefore, in single sided scanning pattern, several hundred micro-seconds of fly-back time is required to reset the scanner to the original position before the scan steps into next position [27]. For a high-speed OCT system (≥200 kHz), the fly-back can be half of the total scanning time depending on the scanning size and density. In such cases the effective duty cycle is only 50% [28], so half of the total scan time is wasted. Many scanning patterns have been developed to eliminate fly-back and increase scanning speed and efficiency. Examples include Lissajous scanning [21], constant linear velocity spiral scanning [29], and constant angular velocity spiral scanning [30]. However, these methods all require an additional step to resample the image into Cartesian coordinates, which increases the complexity of image post-processing. A bidirectional scanning protocol (Fig. 2) using a triangular function on the fast-axis has been developed recently on a 200-kHz SS-OCT system [20]. The forward scanning and the backward scanning are consecutively acquired without the use of fly-back scans. By applying this scheme, the scan duty cycle is increased to almost 100%.
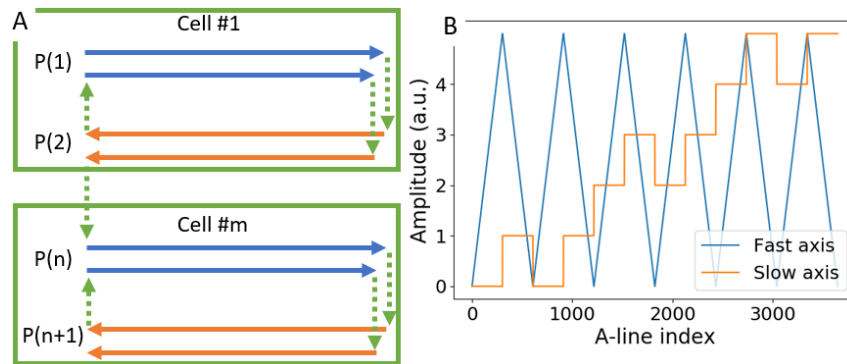

Fig. 2. Example of one bidirectional scanning protocol. (A) Scanning cells contain the lateral positions P(1), P(2), …, P(n), P(n + 1) swept during OCTA data acquisition. The first scanning position of the second cell is acquired after the positions in the previous cells have been scanned two times. Orange arrows and blue arrows indicate different scanning position, (B) Details of the voltage signal applied to each galvanometer.

2.4 Bidirectional scanning protocols sustain reasonable time delay and efficiency for high-speed OCTA

Considering that the optimal time delay between B-scans is around 3-5 ms for OCTA of capillary blood flow [11], in higher speed OCT systems using conventional raster scans the number of A-lines acquired in each B-scan has to be very large to ensure a reasonable scan

interval. Although this results in a higher A-line density sampling, it does not necessarily translate into better lateral resolution, which is fundamentally limited by numerical aperture of the eye and ocular aberrations. Moreover, high speed systems also demand that the raster scanning pattern dedicate the same amount of time and therefore more A-lines per B-scan to the fly-back portion in order to avoid mechanical damage on the scanning hardware. For these reasons the conventional raster scanning pattern is an inefficient option. Conversely, a bidirectional scan pattern can be adapted to reasonable B-scan time delays by increasing the number of positions along slow-axis positions acquired within one unit (Fig. 3). For example, the B-scan interval can be doubled by combining four positions into one scanning unit (Fig. 3(A), (B)); and tripled by combining six positions into one scanning unit (Fig. 3(C), (D)) [20], depending on the needs imposed by the A-scan rates of the system.
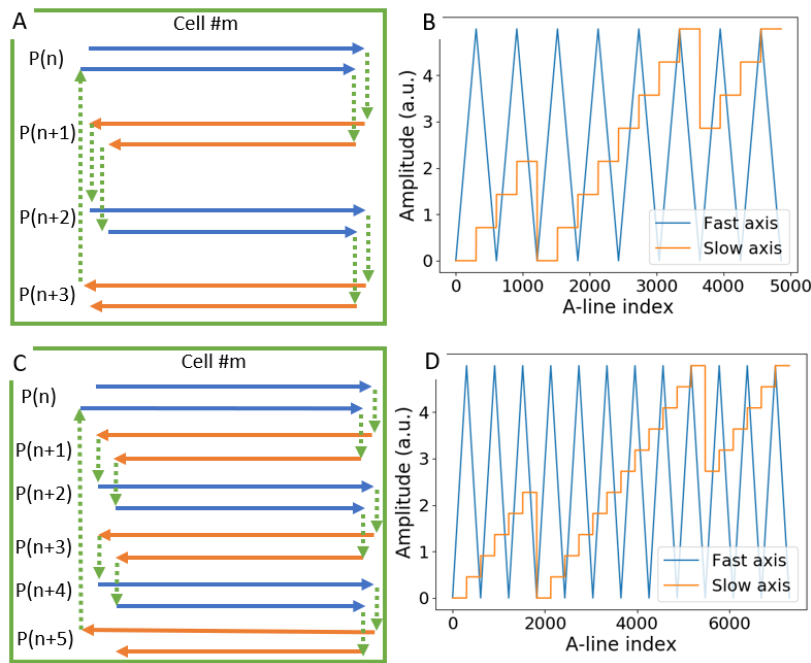

Fig. 3. Example of a protocol based on combined bidirectional scanning cells. (A) A basic cell containing four scanning positions, P(n) to P(n + 3). (B) Voltage signal applied on galvo mirrors for the four scanning position configurations. (C) A basic cell containing six scanning positions, P(n) to P(n + 5). (D) Voltage signal applied on galvo mirrors for the six-scanning position configuration.

2.5 Bidirectional, interleaved scanning patterns achieve HDR-OCTA

As discussed in section 2.1, the flow dynamic range depends on the B-scan time interval. Conventional, equal interval scanning patterns have only one single, fixed scanning interval between two scans repetitions at a location. If multiple scanning intervals are desired, the number of repetitions should be carefully considered, since the number of repeated scans also determines the total time for completing a single scan volume. For a fixed scan interval, the number of repetitions at a location must exceed the number of different scanning intervals, since a scan interval will always be encapsulated by two scans. However, by carefully choosing different scan interval lengths, this limit can be bypassed. For variable length scan intervals, the total number of scan intervals N_{interval} that are constructed from $N_{\text{B-scan}}$ of B-scans can be calculated from the binomial coefficient as

$$N_{\text{interval}} = \begin{pmatrix} N_{B-scan} \\ 2 \end{pmatrix}. \qquad (6)$$
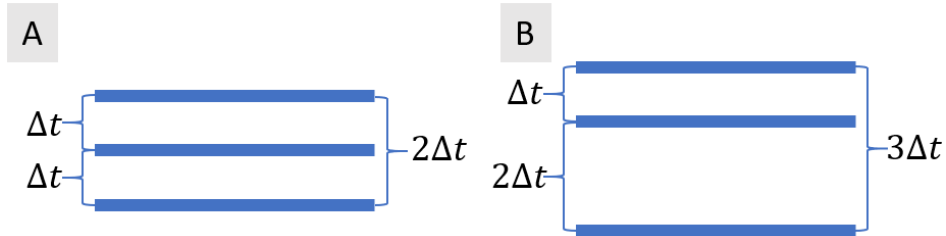

Fig. 4. (A) conventional equal interval scanning method, for which the total number of intervals available for measurements is two, corresponding to Δt and $2\Delta t$. (B) interleaved scanning achieves the number of scan intervals from the same number of scans, as given by Eq. (6). In this case, 3 different scanning intervals ($\Delta t, 2\Delta t, \text{and} 3\Delta t$) are obtained from 3 B-scans.

The total number of scan intervals, N_{interval} , is not just number of different intervals between adjacent scans, since non-adjacent repetitions can also be used to construct a different scan interval. So, for example, if we have three repetitions, the total number of different scanning intervals we can construct from equal interval scans is two (Fig. 4(A)). However, if we make the second scanning interval twice the duration of the first scanning interval, we end up with 3 total scan intervals (Fig. 4(B)).
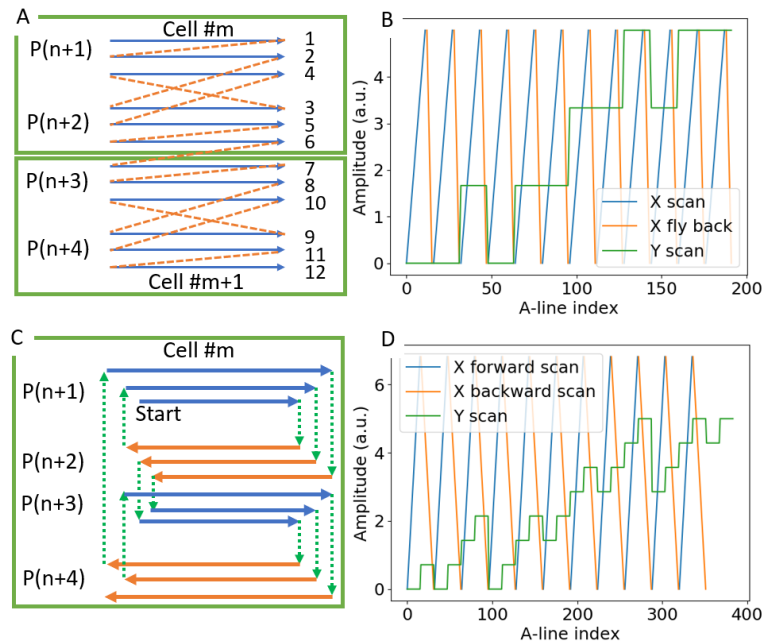

Fig. 5. (A) Diagram to show the raster scan based HDR-OCTA scan pattern at different positions P(n). Orange lines indicated flyback movements (B) Signal applied to the galvo scanner. (C) Bidirectional HDR-OCTA scanning pattern. (D) signal applied to the galvo scanner for the HDR-OCTA scan pattern. X axis is the fast axis, Y axis is the slow axis.

To achieve this, a special scanning sequence is needed. An interleaved raster scanning pattern was designed first to modify the second scanning interval. In this scanning pattern, every two cross-sectional positions form a scanning unit, the scanning pattern in each unit is same. The scanner first scans one position twice and then scans the next position once and

returns back to scan the original position a third time (Fig. 5(A), (B)). By doing so, the second scanning interval from the three repetitions will be twice the duration of the first scanning interval. However, the raster scanning pattern includes non-efficient fly-backs, which are especially problematic on our high-speed system due to limits in galvo motor speed. To overcome this problem, we developed a bidirectional HDR-OCTA scanning pattern (Fig. 5(C), (D)). In our scanning protocol, the time between the first and second repetition is different than the time between second and third repetition, allowing a total of 3 different inter-scan times (1-2, 2-3 and 1-3). The larger number of interscan times improves the dynamic range of the system and the *in vivo* HDR scan can be acquired in less than two seconds. This minimizes the prevalence of motion artifacts, which are more predominant in the scanning intervals most sensitive to slow speed flow.

2.6 Flow phantom experiment

As indicated in Eq. (5), the flow and OCTA signal have an exponential relationship. This relationship has been measured in our previous studies [10]. Previous work has demonstrated the *in vivo* OCTA dynamic range can be expanded by applying different scanning intervals [16], however it is difficult to quantify dynamic range *in vivo*. To study the dynamic range change resulting from different scanning intervals and patterns quantitatively we designed a flow phantom experiment. We used a flow phantom connected to a syringe pump that can be set to different flow rates. A 250 µm inner diameter glass tubing was used here. It was placed on a paper board and then sealed using hot melt glue. Hot melt glue, as a semitransparent material, can be treated as background tissue. The blood sample used in the tubing is bovine blood (Carolina Biological Supply Company). The flow speed was manually set from 0 to 6 mm/s, with steps of 0.3 mm/s. The whole experiment setup and the OCT system sample arm were placed on an air insulated optical table to prevent the vibrations.

3. Results

3.1 Dynamic range can be expanded using HDR-OCTA

A flow phantom cross-sectional image was acquired in a single location. 128 B-scans were acquired. In the acquired data set, the scanning intervals between adjacent B-scan of 1.5 ms; the interval between every two B-scan is 3 ms, and the interval between every three B-scan is 4.5 ms. From this data set it is possible to construct a total of 125 OCTA B-scans at the longest time (since the last 3 scans lack additional scans that could be used to obtain a 4.5 ms interval). Using this data set we calculated the flow value D by averaging over the tubing area in each OCTA B-scan. Each data set contains 125 decorrelations. From these, the mean decorrelation value $\overline{D}$ was calculated. In Fig. 6, we plot $\overline{D}$ corresponding to different flow speeds and fit using Eq. (5). The data follows the theoretical prediction (Fig. 6(A)). Additionally, we define thresholds for the dynamic range of our system according to these measurements. The lower threshold for each scanning interval is defined using the minimum of the decorrelation value D_{min} plus the standard deviation of the decorrelation values D_{std} of each data set (Eq. (7)).

$$D_{std} = std(D) \tag{7}$$

The upper threshold decorrelation value is defined analogously, but by subtracting D_{std} from the averaged saturated decorrelation values, D_{max}. That is, for an upper threshold T_u (Eq. (8)) and a lower threshold T_l (Eq. (9)) we have

$$T_u = D_{max} - D_{std} \tag{8}$$

$$T_l = D_{min} + D_{std} \tag{9}$$

The upper threshold and the lower threshold were overlapped across three different scanning intervals. The overlapping threshold is expected, which is only depended on the sensitivity of the detector. According to this flow phantom experiment, the dynamic range is improved by 25% by applying the multi-scanning interval (Fig. 6(B)).
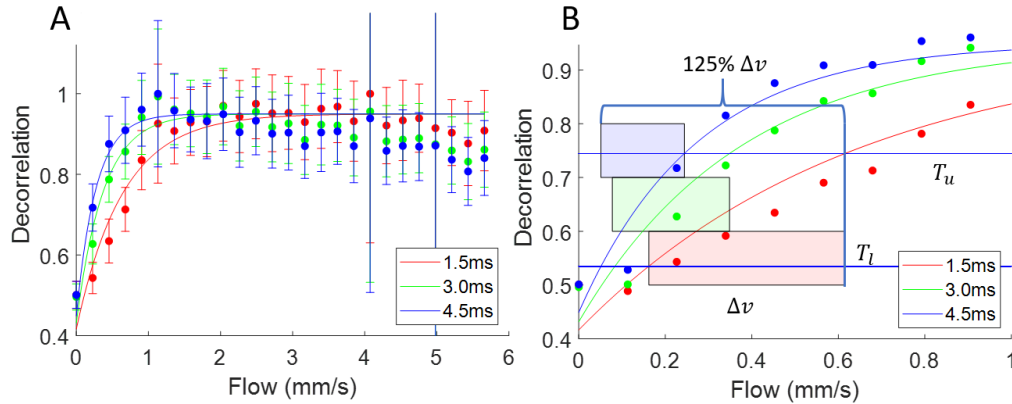

Fig. 6. (A) Fitted flow phantom experiment results at different scanning intervals and flow speeds, (B) Dynamic range calculated using experimental data. The shaded rectangular boxes indicate the dynamic range of different scanning intervals. Δv : dynamic range of 1.5 interval, dynamic range after combining three intervals is increased by 125%. T_u : upper threshold, T_l : lower threshold.

3.2 In vivo retinal imaging

Five healthy human retinal images were acquired using a 400-kHz swept-source OCT system by an experienced OCT operator. The data sets have 304 A-line per B-scan and 912 B-scans with 3 repeats per volume. The total scanning time for each volume is 2 seconds. The scanning size is 3×3 mm^2. In the slow axis direction, the data was over sampled to improve the signal to noise ratio. Both macular and optic nerve head regions were acquired. Three different scanning intervals 1.5 ms, 3 ms and 4.5 ms were generated in single data set. The data was processed using the SSADA algorithm with eleven split spectra. We are assuming there is minimal motion in the fast axis scan, so during our data processing we didn't apply any registration in the fast axis direction. The images were then segmented using our automatic segmentation software [31]. The inner retina *en face* projection images were generated using the maximum projection from the internal limiting membrane (ILM) to the outer plexiform layer (OPL) [32]. All the *en face* images were normalized according to the maximum and minimum values. A 2x2 median filter was applied to reduce the background noise. A custom angiogram colormap was applied to the images to improve the vessel contrast. This color map is a linear, and the same color scales are applied to all the images for fair comparison. The combined images were generated after we applied a fixed threshold to each *en face* image from different scanning intervals. In the peripapillary retinal angiograms, the 1.5 ms and 3 ms images show less capillary structure than the 4.5 ms image, but the 4.5 ms image has more noise than the 1.5 ms and 3 ms images. The combined image is generated by adding three images together. The combined HDR-OCTA image demonstrates the best capillary visibility and has least noise (Fig. 7).
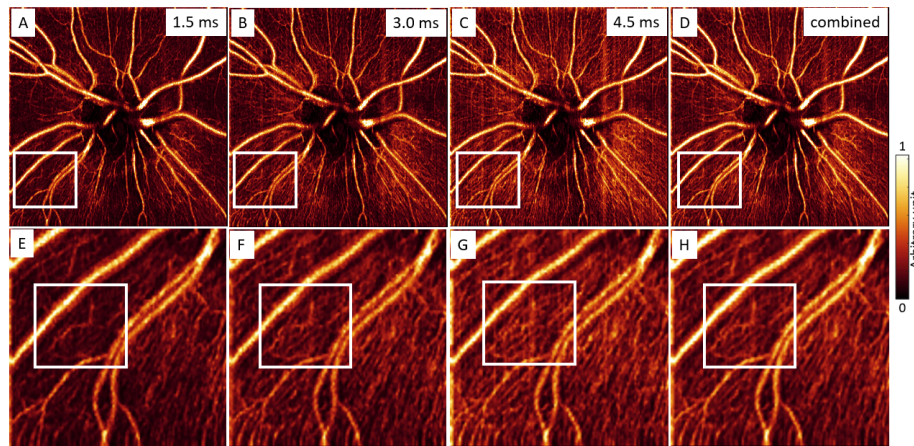
Fig. 7. Human peripapillary retina images. (A-C) three different scanning interval images with three different dynamic ranges. (D) combined HDR-OCTA image. The white box in A, B, C and D is expanded in E, F, G and H. The region in E, F, G and H that is highlighted using another white box shows significant different between the different intervals.

In the macular retina, there is less variation in blood flow velocity, and it is difficult to distinguish the change between different scanning intervals. Here, we calculated the decorrelation signal to noise ratio (DSNR) of each individual image [1]. The DSNR is increasing as the scanning interval becomes longer. The combined image has the largest DSNR. In our macular angiograms (Fig. 8), we can also see that the 1.5 ms image has less capillary structure than the 4.5 ms one, and the 4.5 ms image has more noise than the 1.5 ms image. The combined image shows more details from the capillaries and at the same time has a lower noise level.
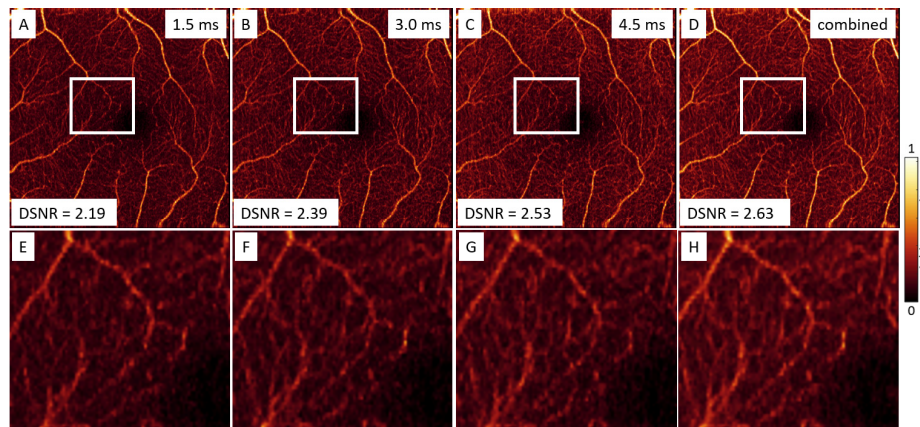

Fig. 8. Human macular retina images. (A-C) three different scanning interval images with three different dynamic ranges. (D) combined HDR-OCTA. The white box in A, B, C and D are expanded in E, F, G and H.

4. Discussion

In this study, we developed a scanning pattern for high speed OCTA data acquisition that increases the dynamic range of flow measurements in the efficient way, thereby achieving this with the less total scan duration. In the *in vitro* study we found an increase of 25% in the dynamic range of flow measurements compared to a conventional raster scan pattern, and *in vivo* measurements indicate that our method successfully removes noise and can potentially allow additional quantification of flow magnitude in retinal images. Future studies that could

explore the link between flow magnitude and pathology must wait for instruments with high dynamic ranges; HDR-OCTA represents an important step in that direction. And, without regard to pathology, there are also basic research questions that measurements of flow magnitude can address.

This work is not the first to consider widening the dynamic range of OCTA measurements [11,16,33]. One method, VISTA, is based on the analysis of the OCTA data from different scanning intervals to extract relative flow information [11,16]. Because of the application of multi-scanning intervals, the flow dynamic range of VISTA is broader than the dynamic range from a single scanning interval. Another method, OCTA Ratio Analysis (OCTARA), is aiming to improve the low flow sensitivity by combining the ratio analysis result from different scanning intervals [33]. These methods both applied the multi-interval mechanism and their dynamic ranges of the combined results are broader than the single ratio analysis results. This study still represents a step forward. HDR-OCTA provides the optimal scan pattern for three B-scan repeats. The efficiency of this scan pattern is significant because it enables growth of the dynamic range of OCTA scans without sacrificing total scan duration. Compared to previous works, this study contributes a method capable of capturing the same dynamic range with less total scanning time. This is going become more important as the speed of commercial and experimental systems continues to grow, both because the returns on scan efficiency will be greater, and because the potential increase in dynamic range will be larger.

The current study was limited to an investigation of an optimal scanning pattern for 3 B-scans at a single location. The interleaved scanning pattern allows measurement of flow from three different scanning intervals using this approach, but our experimental results showed that this number of scan repetitions is limited to an increase of 25% in flow signal dynamic range. To further extend the dynamic range further; it will require more scan repetitions at a single location; however, with faster OCT systems more repetitions become more plausible. The drawback of using a faster system is a requirement for a high-performance scanner. Since we are using a complicated scanning pattern, the galvo scanner and its driver need to be tuned to make sure it has the minimum response time. A long response time will cause vibration when galvo scanner changes moving direction. In the future, the trade-off between scan volume acquisition time and dynamic range as parametrized by number of repeats could be explored. Defining the contours of this relationship would allow the clinical community to decide on the number of repetitions based on the needs of personalized care for specific diseases. In addition to this potential future study, it will be useful to extend HDR-OCTA into wide field imaging regimes. The variation in flow speed is more pronounced between different regions of the retina, so the benefit of measuring this variation will be more pronounced in wide field systems. As OCT technology as a whole moves in this direction [34–36], HDR-OCTA represents a promising, complimentary addition to other extensions of the technology.

5. Conclusion

The dynamic range of OCTA is a key factor that limits the sensitivity to flow change. In this paper, a bidirectional scanning pattern was explored and compared with the conventional raster scan pattern. A novel interleaved scanning pattern was successfully developed for both raster and bidirectional scanning methods. The results from a flow phantom experiment quantitatively verified the possibility of expanding the dynamic range through a multi-interval scanning method. *In vivo* human peripapillary and macular images were also successfully acquired using the bidirectional interleaved scan pattern. The improvement of dynamic range was verified by comparing OCTA images with three different intervals and the final combined image (HDR-OCTA).

Funding

Disclosures

Oregon Health & Science University (OHSU) and Yali Jia have a significant financial interest in Optovue, Inc. These potential conflicts of interest have been reviewed and managed by OHSU.

References

1. Y. Jia, O. Tan, J. Tokayer, B. Potsaid, Y. Wang, J. J. Liu, M. F. Kraus, H. Subhash, J. G. Fujimoto, J. Hornegger, and D. Huang, "Split-spectrum amplitude-decorrelation angiography with optical coherence tomography," Opt. Express **20**(4), 4710–4725 (2012).
2. L. An and R. K. Wang, "In vivo volumetric imaging of vascular perfusion within human retina and choroids with optical micro-angiography," Opt. Express **16**(15), 11438–11452 (2008).
3. S. Makita, Y. Hong, M. Yamanari, T. Yatagai, and Y. Yasuno, "Optical coherence angiography," Opt. Express **14**(17), 7821–7840 (2006).
4. A. Mariampillai, B. A. Standish, E. H. Moriyama, M. Khurana, N. R. Munce, M. K. Leung, J. Jiang, A. Cable, B. C. Wilson, I. A. Vitkin, and V. X. Yang, "Speckle variance detection of microvasculature using swept-source optical coherence tomography," Opt. Lett. **33**(13), 1530–1532 (2008).
5. L. A. Yannuzzi, K. T. Rohrer, L. J. Tindel, R. S. Sobel, M. A. Costanza, W. Shields, and E. Zang, "Fluorescein angiography complication survey," Ophthalmology **93**(5), 611–617 (1986).
6. J. Fingler, D. Schwartz, C. Yang, and S. E. Fraser, "Mobility and transverse flow visualization using phase variance contrast with spectral domain optical coherence tomography," Opt. Express **15**(20), 12636–12653 (2007).
7. X. Wei, A. Camino, S. Pi, W. Cepurna, D. Huang, J. C. Morrison, and Y. Jia, "Fast and robust standard-deviation-based method for bulk motion compensation in phase-based functional OCT," Opt. Lett. **43**(9), 2204–2207 (2018).
8. T. Klein, W. Wieser, C. M. Eigenwillig, B. R. Biedermann, and R. Huber, "Megahertz OCT for ultrawide-field retinal imaging with a 1050 nm Fourier domain mode-locked laser," Opt. Express **19**(4), 3044–3062 (2011).
9. A. Agrawal, T. J. Pfefer, P. D. Woolliams, P. H. Tomlins, and G. Nehmetallah, "Methods to assess sensitivity of optical coherence tomography systems," Biomed. Opt. Express **8**(2), 902–917 (2017).
10. J. P. Su, R. Chandwani, S. S. Gao, A. D. Pechauer, M. Zhang, J. Wang, Y. Jia, D. Huang, and G. Liu, "Calibration of optical coherence tomography angiography with a microfluidic chip," J. Biomed. Opt. **21**(8), 86015 (2016).
11. W. Choi, E. M. Moult, N. K. Waheed, M. Adhi, B. Lee, C. D. Lu, T. E. de Carlo, V. Jayaraman, P. J. Rosenfeld, J. S. Duker, and J. G. Fujimoto, "Ultrahigh-speed, swept-source optical coherence tomography angiography in nonexudative age-related macular degeneration with geographic atrophy," Ophthalmology **122**(12), 2532–2544 (2015).
12. B. Braaf, K. A. Vermeer, K. V. Vienola, and J. F. de Boer, "Angiography of the retina and the choroid with phase-resolved OCT using interval-optimized backstitched B-scans," Opt. Express **20**(18), 20516–20534 (2012).
13. R. F. Spaide, J. G. Fujimoto, N. K. Waheed, S. R. Sadda, and G. Staurenghi, "Optical coherence tomography angiography," Prog. Retin. Eye Res. **64**, 1–55 (2018).
14. P. L. Nesper, P. K. Roberts, A. C. Onishi, H. Chai, L. Liu, L. M. Jampol, and A. A. Fawzi, "Quantifying microvascular abnormalities with increasing severity of diabetic retinopathy using optical coherence tomography angiography," Invest. Ophthalmol. Vis. Sci. **58**(6), BIO307 (2017).
15. G. Lutty, J. Grunwald, A. B. Majji, M. Uyama, and S. Yoneya, "Changes in choriocapillaris and retinal pigment epithelium in age-related macular degeneration," Mol. Vis. **5**, 35 (1999).
16. S. B. Ploner, E. M. Moult, W. Choi, N. K. Waheed, B. Lee, E. A. Novais, E. D. Cole, B. Potsaid, L. Husvogt, and J. Schottenhamml, "Toward quantitative OCT angiography: visualizing blood flow speeds in ocular pathology using variable interscan time analysis (VISTA)," Retina **36**, S118–S126 (2016).
17. R. Szeliski, *Computer Vision: Algorithms and Applications* (Springer Science & Business Media, 2010).
18. R. K. Mantiuk, K. Myszkowski, and H. P. Seidel, "High dynamic range imaging," *Wiley Encyclopedia of Electrical and Electronics Engineering* (Wiley, 1999), pp. 1–42.
19. M. Szkulmowski, I. Gorczynska, D. Szlag, M. Sylwestrzak, A. Kowalczyk, and M. Wojtkowski, "Efficient reduction of speckle noise in Optical Coherence Tomography," Opt. Express **20**(2), 1337–1359 (2012).
20. M. J. Ju, M. Heisler, A. Athwal, M. V. Sarunic, and Y. Jian, "Effective bidirectional scanning pattern for optical coherence tomography angiography," Biomed. Opt. Express **9**(5), 2336–2350 (2018).
21. Y. Chen, Y.-J. Hong, S. Makita, and Y. Yasuno, "Three-dimensional eye motion correction by Lissajous scan optical coherence tomography," Biomed. Opt. Express **8**(3), 1783–1802 (2017).

22. I. Grulkowski, I. Gorczynska, M. Szkulmowski, D. Szlag, A. Szkulmowska, R. A. Leitgeb, A. Kowalczyk, and M. Wojtkowski, "Scanning protocols dedicated to smart velocity ranging in spectral OCT," Opt. Express **17**(26), 23736–23754 (2009).

23. F. Jaillon, S. Makita, and Y. Yasuno, "Variable velocity range imaging of the choroid with dual-beam optical coherence angiography," Opt. Express **20**(1), 385–396 (2012).

24. S. S. Gao, G. Liu, D. Huang, and Y. Jia, "Optimization of the split-spectrum amplitude-decorrelation angiography algorithm on a spectral optical coherence tomography system," Opt. Lett. **40**(10), 2305–2308 (2015).

25. A. Fercher and J. D. Briers, "Flow visualization by means of single-exposure speckle photography," Opt. Commun. **37**(5), 326–330 (1981).

26. X. Wei, A. Camino, S. Pi, T. T. Hormel, W. Cepurna, D. Huang, J. C. Morrison, and Y. Jia, "Real-time cross-sectional and en face OCT angiography guiding high-quality scan acquisition," Opt. Lett. **44**(6), 1431–1434 (2019).

27. V.-F. Duma, K. S. Lee, P. Meemon, and J. P. Rolland, "Experimental investigations of the scanning functions of galvanometer-based scanners with applications in OCT," Appl. Opt. **50**(29), 5735–5749 (2011).

28. V.-F. Duma, P. Tankam, J. Huang, J. Won, and J. P. Rolland, "Optimization of galvanometer scanning for Optical Coherence Tomography," Appl. Opt. **54**(17), 5495–5507 (2015).

29. O. M. Carrasco-Zevallos, C. Viehland, B. Keller, R. P. McNabb, A. N. Kuo, and J. A. Izatt, "Constant linear velocity spiral scanning for near video rate 4D OCT ophthalmic and surgical imaging with isotropic transverse sampling," Biomed. Opt. Express **9**(10), 5052–5070 (2018).

30. L. Huo, J. Xi, Y. Wu, and X. Li, "Forward-viewing resonant fiber-optic scanning endoscope of appropriate scanning speed for 3D OCT imaging," Opt. Express **18**(14), 14375–14384 (2010).

31. Y. Guo, A. Camino, M. Zhang, J. Wang, D. Huang, T. Hwang, and Y. Jia, "Automated segmentation of retinal layer boundaries and capillary plexuses in wide-field optical coherence tomographic angiography," Biomed. Opt. Express **9**(9), 4429–4442 (2018).

32. T. T. Hormel, J. Wang, S. T. Bailey, T. S. Hwang, D. Huang, and Y. Jia, "Maximum value projection produces better *en face* OCT angiograms than mean value projection," Biomed. Opt. Express **9**(12), 6412–6424 (2018).

33. P. E. Stanga, E. Tsamis, A. Papayannis, F. Stringa, T. Cole, and A. Jalil, "Swept-source optical coherence tomography angio (Topcon Corp, Japan): technology review," in *OCT Angiography in Retinal and Macular Diseases* (Karger Publishers, 2016), pp. 13–17.

34. G. Liu, J. Yang, J. Wang, Y. Li, P. Zang, Y. Jia, and D. Huang, "Extended axial imaging range, widefield swept source optical coherence tomography angiography," J. Biophotonics **10**(11), 1464–1472 (2017).

35. P. Zang, G. Liu, M. Zhang, C. Dongye, J. Wang, A. D. Pechauer, T. S. Hwang, D. J. Wilson, D. Huang, D. Li, and Y. Jia, "Automated motion correction using parallel-strip registration for wide-field en face OCT angiogram," Biomed. Opt. Express **7**(7), 2823–2836 (2016).

36. W. Drexler, M. Liu, A. Kumar, T. Kamali, A. Unterhuber, and R. A. Leitgeb, "Optical coherence tomography today: speed, contrast, and multimodality," J. Biomed. Opt. **19**(7), 071412 (2014).